HHS Public Access

Author manuscript

J Neurosurg. Author manuscript; available in PMC 2024 July 01.

Published in final edited form as:

J Neurosurg. 2023 July 01; 139(1): 150–156. doi:10.3171/2022.11.JNS222213.

Benchtop Proof of Concept and Comparison of Iron and Magnesium Based Bioresorbable Flow Diverters

Alexander A. Oliver, BS[1,2,3], **Cem Bilgin, MD**[2], **Andrew J. Vercnocke, BS**[2], **Kent D. Carlson, PhD**[3], **Ramanathan Kadirvel, PhD**[2,4], **Roger J Guillory II, PhD**[5], **Adam J. Griebel, MS**[6], **Jeremy E. Schaffer, PhD**[6], **Dan Dragomir-Daescu, PhD**[1,3], **David F. Kallmes, MD**[1,2]

[1]Biomedical Engineering and Physiology, Mayo Clinic Graduate School of Biomedical Sciences, Rochester, Minnesota, USA

[2]Radiology, Mayo Clinic, Rochester, Minnesota, USA

[3]Physiology and Biomedical Engineering, Mayo Clinic, Rochester, Minnesota, USA

[4]Neurosurgery, Rochester, Minnesota, USA

[5]Biomedical Engineering, Michigan Technological University, Houghton, Michigan, USA

[6]Fort Wayne Metals, Fort Wayne, Indiana, USA

Abstract

Objective: Bioresorbable flow diverters (BRFDs) could significantly improve the performance of next generation flow diverter technology. In the current work, magnesium and iron alloy BRFDs are prototyped and compared in terms of porosity/pore density, radial strength, flow diversion functionality, and resorption kinetics to offer insights into selecting the best available bioresorbable metal candidate for the BRFD application.

Methods: BRFDs were braided out of magnesium (MgBRFD) or iron (FeBRFD) alloy wires. Pore density and crush resistance force were measured using established methods. BRFDs were deployed in silicone aneurysm models attached to flow loops to investigate flow diversion functionality and resorption kinetics in a simulated physiological environment.

Results: The FeBRFD exhibited higher pore density (9.9 vs 4.3 pores/mm^2) and crush resistance force (0.69±0.05 vs 0.53±0.05 N/cm, p = 0.0765, n = 3 per group) than the MgBRFD, although both crush resistances were within the range previously reported for FDA approved flow diverters. The FeBRFD demonstrated greater flow diversion functionality than MgBRFD, with significantly higher values of established flow diversion metrics (Mean transit time: 159.6±11.9 vs 110.9±1.6, p = 0.015; Inverse wash-out slope: 192.5±9.0 vs 116.5±1.5, p = 0.001; n = 3 per group; both metrics expressed as a percentage of the control condition). Lastly, the FeBRFD was able to maintain its braided structure for >12 weeks, whereas the MgBRFD was almost completely resorbed after 5 weeks.

Corresponding Author's name and current institution: Alexander A. Oliver, Mayo Clinic, Oliver.Alexander@mayo.edu, aaoliver@mtu.edu.

Previous Presentations: This work has not been previously presented.

Conclusions: We have demonstrated the ability to manufacture BRFDs out of magnesium and iron alloys. Our data suggests that the iron alloy is the superior material candidate for the BRFD application due to its higher mechanical strength and lower resorption rate relative to the magnesium alloy.

Keywords

Flow Diverter; Bioresorbable; Bioabsorbable; Absorbable; Biodegradable; Stent

Introduction:

Flow diverters (FDs) are a rapidly growing endovascular approach for the treatment of intracranial aneurysms due to their relatively good safety profiles and high aneurysm occlusion rate in the clinic[1]. While FDs represent an advancement in the endovascular treatment of intracranial aneurysms, there are several drawbacks associated with these devices. All FDA approved FDs are composed of permanent metals that will remain in the patient for the duration of their life[2]. Some drawbacks of FDs include device induced thromboembolism[3,4], stenosis of the parent artery[5–7], and occlusion of adjacent branching arteries[1]. Bioresorbable flow diverters (BRFDs) have been proposed by several independent investigators as the next generation of FD technology to combat some of these drawbacks[8]. The ideal BRFD serves its transient function of healing and occluding the aneurysm prior to being safely resorbed by the body, mitigating complications associated with the permanent presence of conventional FDs. Proposed advantages of BRFDs over conventional FDs include: reductions in device induced 1) thromboembolism, 2) chronic inflammation and stenosis, 3) side branch occlusion, 4) medical imaging artifacts, plus 5) restoration of physiological vasomotor function, and 6) use in pediatric applications[8].

While the concept of BRFDs is relatively new, bioresorbable stents have been extensively studied for coronary applications and have showcased the feasibility, safety, and advantages of bioresorbable vascular scaffolds in the clinic[9]. Both metallic[9] and polymeric[10] bioresorbable coronary stents have been evaluated on the lab bench and in the clinic. These studies have demonstrated that the intrinsically higher mechanical strength and stiffness of bioresorbable metals, as well as their high ductility and biocompatibility, favors them for use as a vascular scaffold over polymers[9,11–14]. Magnesium (Mg) and iron (Fe) alloys are the two most developed classes of bioresorbable metals. Mg-based bioresorbable stents have achieved market approval in Europe and demonstrated promising results in an ongoing post market trial of over 2000 patients[15,16]. Fe-based bioresorbable stents are involved in ongoing clinical trials in China and so far have demonstrated good safety profiles and minimal restenosis out to 26 months[17]. Based on the success of bioresorbable metals compared to polymers in the similar stenting application, we are motivated to develop and investigate metallic BRFDs.

In the current work, we prototype BRFDs using Mg (MgBRFD) and Fe (FeBRFD) alloys, and we demonstrate the feasibility of using metals for BRFD applications. MgBRFD and FeBRFDs are compared in terms of porosity/pore density, radial strength, flow diversion

functionality, and resorption kinetics to offer insights into which bioresorbable metal candidate is better for the current BRFD application.

Methods:

Devices

Prototype BRFDs with diameters of 4.75 mm were fabricated for this study. Due to the anticipated lower strength and stiffness and faster resorption of the Mg alloy wires, a larger diameter was selected for the Mg alloy wires than the Fe alloy wires. This larger wire diameter required a reduced wire count due to geometrical constraints during manufacturing.

The MgBRFDs contained 32 wires braided at ~60°. Of the 32 wires, 24 wires were composed of a bioresorbable Mg alloy, WE22 (Fort Wayne Metals, Fort Wayne, IN), which contained >95% Mg and the rest rare earth elements by weight percentage. The WE22 wires had a diameter of 50 μm. The remaining 8 wires were composed of tantalum (Ta) for radio-opacity during device delivery and were 30 μm in diameter. The Ta wires were coated to a diameter of 40 μm with polyimide to prevent galvanic corrosion at the Mg-Ta interface.

The FeBRFDs contained 48 wires also braided at ~60°. Of the 48 wires, 36 were composed of an antiferromagnetic bioresorbable Fe alloy, FeMnN (Fort Wayne Metals, Fort Wayne, IN), which contained 35% manganese, 0.15% nitrogen, and the balance Fe by weight percentage[18]. The FeMnN wires had a diameter of 25 μm. The smaller diameter wires allowed us to incorporate more total wires into the braid during manufacturing. The remaining 12 wires were composed of the polyimide coated Ta described above.

Both sets of materials were braided onto 4.75 mm mandrels in 1 m long segments and heat treated by Fort Wayne Metals. Braids were then cut to desired lengths for each experiment described below. Both wire subcomponents were manufactured by Fort Wayne Metals.

Porosity and Pore Density

Images of both devices were taken with a stereomicroscope (Leica MZ 125) at 4 times normal magnification. Porosity and pore density measurements were taken from a 2.5 × 6 mm region of the images centered about the top of the device. Porosity and pore density were quantified using the imbinarize function in MATLAB (MathWorks Inc., Natick, MA, USA). Porosity is defined as (empty area / total area) × 100%. Pore density is defined as number of complete pores per mm^2 as previously described[19]. Braid angle was measured from the same images using imageJ.

Crush Resistance Testing

MgBRFD and FeBRFDs were cut to 10 mm in length. The devices were placed between two parallel plates connected to a linear motion stage (Z825B actuator, KST101 controller, Thorlabs). One plate was fixed, and the other was translated at a speed of 0.1 mm/s, crushing the BRFDs from their nominal diameter to a diameter of approximately 1 mm, and then the translated plate was returned to its original position. For the duration of stage translation, the radial force exerted by the BRFD was measured using a 2.5lb load cell (MDB2.5, Transducer Techniques). Radial force was then plotted against device diameter. The crush

resistance force is defined as the force required to crush the BRFD to 50% of its nominal diameter, as previously described[19,20]. Three replicate devices were tested for each device type.

In Vitro Flow Diversion

MgBRFD or FeBRFDs were cut to 15 mm in length and deployed in a 3D printed sidewall aneurysm model (Formlabs, Elastic50a resin) with a parent vessel ID of 4.5 mm, aneurysm neck of 5.2 mm, and height and width of 8 mm. The parent vessel curved 160° around a 10 mm radius and the aneurysm was placed at the apex of the curve. The model was then attached to a peristaltic pump and water was pumped through the system at a mean flow rate of 4.5 mL/s. A 6 mL bolus of Omnipaque contrast was injected at a rate of 4 mL/s using a power injector. A 20 second digital subtraction angiography cine at 30 frames/s was taken using a Siemens Artis angiography (Siemens Healthineers, Erlangen, Germany) to record the flow of contrast into and out of the aneurysm. This was performed in 3 replicates for aneurysm models containing no devices (control), a MgBRFD, or an FeBRFD. Each recording was uploaded into MATLAB for analysis. The region of interest (ROI) was defined as the aneurysm sac. The average grayscale value in the ROI for each frame was plotted over time to form a time density curve (TDC), as previously described[21,22]. Each TDC was normalized such that the peak, corresponding to maximum contrast within the aneurysm, had a value of 1 and no contrast within the aneurysm had a value of 0. Three parameters were calculated for each TDC: 1) Mean transit time (MTT) – the time coordinate associated with the centroid of the area under the TDC; 2) Wash-in slope (WIS) – the slope of the TDC from initial time of contrast entering the aneurysm to peak intensity; and 3) Wash-out slope (WOS) – the slope of the TDC from peak contrast intensity to complete contrast wash out or minimum contrast intensity within the aneurysm, all as previously defined[21,22]. Greater MTT, lower WIS, and lower WOS are associated with better flow diversion[21]. Therefore, MTT, WIS^{-1}, and WOS^{-1} were plotted and compared between devices so that higher values correspond to increased flow diversion[21,22]. MTT, WIS^{-1}, and WOS^{-1} were expressed for MgBRFD and FeBRFD as percentages of the control condition.

In Vitro Resorption Analysis

The FeBRFDs were sonicated in 15% citric acid for 5 minutes, deionized water for 3 minutes, and then absolute ethanol for 1 minute to remove the thin oxidized surface layer as previously described[14]. MgBRFD and FeBRFDs cut to 10 mm were deployed in 3D printed sidewall aneurysm models (Formlabs, Elastic 50a resin) with a parent vessel inner diameter of 4 mm, an aneurysm neck of 4 mm, and height and width of 8 mm. Three replicates were performed for each device type. Each device containing model was then incorporated into a flow loop attached to a peristaltic pump. Dulbecco's Modified Eagle Media was pumped through each loop at 0.5 mL/s. 30 mL of media was used per device and was changed every 3 days per ASTM G31-72 standard. The flow loop was placed in a 37°C incubator for the duration of the experiment. At 0, 1, 5, and 12 weeks, the device containing models were removed from the flow loop, perfused with media, and imaged using a Bruker SkyScan 1276 micro-CT scanner. The scans were acquired using a 0.25 mm aluminum filter, a source voltage of 55 kV, and a source current of 200 μA. Projection images were taken every 0.2° over a 360° range with an exposure time of 0.48s. The image data was reconstructed using

a modified Feldkamp cone-beam algorithm (NRecon, Bruker) to produce image data with a voxel resolution of 8 μm. Thresholding was based on the manufacturer's specifications of wire diameter for each wire type at time point 0. The microCT scans were used to generate 3D renderings and quantify reductions in device volume over time. Volume reductions are presented as percentages of the original volume of the bioresorbable wires of each device. Following each scan, the devices were returned to the flow loop until the next time point.

Statistical Methods

All testing was performed in 3 replicates per device type. All metrics are presented as the mean ± standard error. Crush resistance force, MTT, WIS^{-1}, and WOS^{-1} are compared between the MgBRFD and FeBRFD using a 2-tailed students T-test assuming equal variance. A linear regression was used to model BRFD volume reduction over time in the in vitro resorption analysis. P-values less than 0.05 were considered statistically significant.

Results:

Porosity and Pore Density

Macroscopic images of the devices are presented in Figure 1(Left). Representative images used to calculate porosity and pore density are presented in Figure 1(Right). The porosity of the MgBRFD and FeBRFDs were 81% and 79%, respectively. The pore density of the MgBRFD and FeBRFDs were 4.3 and 9.9 pores/mm^2, respectively. The lower pore density of the MgBRFD can be attributed to its lower wire count within the braid. The braid angle was 64° for both devices.

Crush Resistance

Radial force plotted against BRFD diameter is presented in Figure 2(Left). Hysteresis was observed in the plots for both device types, where they exhibited a higher force when resisting crush compared to the force they applied to the parallel plates during device reexpansion, which is typical for endovascular devices[20]. Crush resistance force is plotted for the two devices in Figure 2(Right). The MgBRFDs and FeBRFDs had crush resistances of 0.53±0.05 N/cm and 0.69±0.05 N/cm respectively, although this difference was not statistically significant ($p = 0.0765$, $n = 3$ per group). The crush resistances of both BRFDs fall within the previously reported range of 0.31 – 1.15 N/cm for FDA approved FDs[19].

In Vitro Flow Diversion

The TDCs for the MgBRFD and FeBRFDs are presented in Figure 3(Left). Qualitatively, there appears to be no difference in contrast wash into the aneurysm between devices. However, the FeBRFD group resulted in a greater degree of contrast stagnation within the aneurysm and reduced contrast washout relative to the MgBRFD group. MTT, WIS^{-1}, and WOS^{-1} for the MgBRFD and FeBRFDs are presented in Figure 3(Right) as a percentage of the control group. There was no statistical difference between MgBRFD and FeBRFD for WIS^{-1} ($p = 0.486$, $n = 3$ per group). However, the FeBRFDs exhibited a significantly higher MTT ($p = 0.015$, $n = 3$ per group) and WOS^{-1} ($p = 0.001$, $n = 3$ per group) than the MgBRFDs, indicating improved flow diversion metrics for the FeBRFD group. These results are trending with other published studies using these flow diversion metrics, where

MTT and WOS^{-1} seem to exhibit the greatest discrepancies between devices for a given model and WIS^{-1} tends to be more similar between devices[21,22].

In Vitro Resorption Analysis

Representative microCT generated 3D renderings of the MgBRFD and FeBRFDs are presented in Figure 4(Left). Substantial resorption of the Mg alloy wires occurred by 1 week, resulting in a loss of the braided geometry structure of the Mg alloy wires. The Mg alloy wires were essentially completely resorbed by 5 weeks, as depicted visually in Figure 4(Left) and quantitatively as percent volume reduction in Figure 4(Right). The linear regression of the Mg alloy wire volume reduction over time was insignificant ($R^2 = 0.374$, $p = 0.388$). The Fe alloy wires resorbed much slower and consequently the braided Fe alloy wire lattice maintained its structure out to 12 weeks, as shown in Figure 4(Left). The Fe alloy wire volume reduction over time was much slower, as shown in Figure 4(Right). The linear regression was statistically significant ($R^2 = 0.934$, $p = 0.034$) and estimated complete resorption of the wires at ~36 weeks.

Discussion:

In the current study we demonstrated the ability to manufacture braided BRFDs out of Mg and Fe alloy wires. The superior strength and slower resorption rate of the Fe alloy relative to the Mg alloy allowed us to manufacture FeBRFDs with 25 μm diameter wires compared to 50 μm for MgBRFDs. The FeBRFD wire diameter and device radial strength was comparable to FDA approved FDs. The smaller wire diameters in the FeBRFD allowed us to incorporate more wires into the braid, improving pore density and ultimately flow diversion functionality relative to MgBRFDs. Furthermore, even with smaller wire diameters, the FeBRFD was able to maintain its braided structure for 12+ weeks compared to only 1 week for MgBRFD in our in vitro resorption analysis. Taken together, we believe that Fe alloys are the superior material for the BRFD application, where smaller diameter wires are optimal, but the device needs to maintain mechanical integrity long enough for the aneurysm to occlude and heal before significant device resorption.

To date, most groups have focused on the development of polymer based BRFDs. Nishi et al. developed a BRFD composed of braided poly-L-lactic acid wires[23]. The completely polymer construct required balloon angioplasty to achieve suitable wall apposition and resulted in an eccentric distribution of wires over the aneurysm neck when deployed in the rabbit elastase induced aneurysm model, leading to low aneurysm occlusion rates. Wang et al.[24] and Jamshidi et al.[19] countered this problem by incorporating permanent metal reinforcing wires into their bioresorbable polymer braids, which allowed the devices to self-expand without the need for balloon angioplasty. This resulted in a higher aneurysm occlusion rate when the Wang et al. devices were deployed in the rabbit elastase induced aneurysm model and excellent wall apposition when the Jamshidi et al. devices were deployed in the rabbit infrarenal abdominal aorta. However, the inferior mechanical strength of polymers relative to metals is evident in the polymer wire diameters, which were in the 40–50 μm range for all three polymeric BRFDs. Our FeBRFDs leverage the

superior strength of metals to construct BRFDs with smaller 25 μm diameter wires without compromising overall device radial force.

One other group has investigated metallic BRFDs. Nevzati et al.[25] and Gruter et al.[26] deployed bioresorbable Mg alloy devices into a rat abdominal aorta/surgical sidewall aneurysm model. They reported high aneurysm occlusion rates and good safety and biocompatibility profiles of the resorbing device. However, their device appeared to be a laser cut stent, featuring 120 μm struts and a very high porosity and low pore density. The porosity/pore density would likely result in low aneurysm occlusion rates in a more rigorous model like the rabbit elastase induced aneurysm model. Furthermore, the large strut sizes would likely preclude it from treating intracranial aneurysms in the clinic. We have demonstrated the ability to manufacture braided FDs out of bioresorbable metals, which more closely resemble the geometry, deployability, porosity, and pore density of FDA approved FDs.

One limitation of our study was the use of a simplified aneurysm model and peristaltic pump for our in vitro flow diversion analysis, as opposed to patient specific aneurysm model geometries and cardiac cycle mimicking flow systems previously reported[21,22]. However, our simplified approach will be easier to reproduce, and it was still able to demonstrate significant differences in flow diversion performance between devices using established metrics (MTT and WOS^{-1}). While our FeBRFDs demonstrated the ability to divert flow and stagnate contrast within the aneurysm, their pore density could be improved to match FDA approved FDs, which have been reported as at least 18 pores/mm^2[19]. Future FeBRFD designs will feature a tighter braid angle to increase pore density. We will investigate the effect of tightened braid angle on device radial strength and flexibility. The in vitro flow diversion function of these modified FeBRFDs will be compared to FDA approved FDs using this model in future work. Another limitation of our study was the in vitro resorption model, wherein the BRFD surfaces were continuously in contact with the flowing media for the duration of the experiment. In the in vivo environment, the device surface would become immediately covered by a layer of blood proteins and eventually neointimal tissue, thus reducing the resorption rate[27–30]. A slower actual resorption rate may be more favorable for the BRFD application. Although the ideal lifetime for BRFDs is yet to be determined by the field, clinical investigations of conventional FDs have suggested that complete vessel remodeling and mature neointimal covering of the aneurysm neck typically occurs in the 6–12 month period[4]. Another limitation of the resorption analysis was that substantial resorption of the MgBRFDs occurred by one week, making it difficult to mathematically model its volume reduction over time. Multiple volume measurements would need to be taken within the first week of MgBRFD resorption to accurately model volume reduction using this experimental set-up.

Future work will investigate the in vivo resorption rate of the BRFDs. The biocompatibility of similar iron and magnesium alloys on vascular cell types has been previously demonstrated in vitro[14,31]. Future work will comprehensively evaluate the biocompatibility of these materials in vivo in terms of device endothelialization, neointimal hyperplasia, and vascular inflammation. Additionally, we will evaluate device deployability, safety, and efficacy of aneurysm occlusion from the BRFDs using the rabbit elastase induced aneurysm

model[32]. The development of magnesium alloys with increased strength, stiffness, and decreased resorption rate may facilitate the use of smaller diameter wires and improve pore density in future MgBRFD device iterations. The Fe alloy used in FeBRFD is composed of an austenitic material structure, resulting in non-ferromagnetic properties[33]. In theory, this should result in MRI compatibility of the FeBRFD. Future work will also focus on confirming the MRI safety and medical image artifact testing of both BRFDs relative to industry standard controls using 1.5T, 3.0T, and 7.0T field strength clinical MRI scanners.

Conclusions:

We have demonstrated the ability to manufacture braided BRFDs out of bioresorbable Mg and Fe alloys. We believe that bioresorbable Fe alloys are a better material candidate than Mg alloys for the BRFD application due to improved mechanical strength and delayed resorption rate of Fe, which allows for the construction of devices with smaller wire diameters. This ultimately resulted in improved pore density and flow diversion characteristics. Future work will evaluate the efficacy, safety, and resorption behavior of the MgBRFD and FeBRFD in animal models.

Acknowledgments:

The authors would like to acknowledge Dr. Yang Liu for his help with the crush resistance testing equipment and David Morse for his help preparing figures.

References

1. Brinjikji W, Murad MH, Lanzino G, Cloft HJ, Kallmes DF. Endovascular treatment of intracranial aneurysms with flow diverters: a meta-analysis. Stroke. 2013;44(2):442–447. [PubMed: 23321438]
2. Dandapat S, Mendez-Ruiz A, Martínez-Galdámez M, et al. Review of current intracranial aneurysm flow diversion technology and clinical use. Journal of NeuroInterventional Surgery. 2021;13(1):54–62. [PubMed: 32978269]
3. Kallmes DF, Hanel R, Lopes D, et al. International retrospective study of the pipeline embolization device: a multicenter aneurysm treatment study. American Journal of Neuroradiology. 2015;36(1):108–115. [PubMed: 25355814]
4. Becske T, Brinjikji W, Potts MB, et al. Long-term clinical and angiographic outcomes following pipeline embolization device treatment of complex internal carotid artery aneurysms: five-year results of the pipeline for uncoilable or failed aneurysms trial. Neurosurgery. 2017;80(1):40–48. [PubMed: 28362885]
5. Guédon A, Clarençon F, Di Maria F, et al. Very late ischemic complications in flow-diverter stents: a retrospective analysis of a single-center series. Journal of neurosurgery. 2016;125(4):929–935. [PubMed: 26824382]
6. Caroff J, Tamura T, King RM, et al. Phosphorylcholine surface modified flow diverter associated with reduced intimal hyperplasia. Journal of NeuroInterventional Surgery. 2018;10(11):1097–1101. [PubMed: 29511117]
7. Flood TF, van der Bom IM, Strittmatter L, et al. Quantitative analysis of high-resolution, contrast-enhanced, cone-beam CT for the detection of intracranial in-stent hyperplasia. Journal of NeuroInterventional Surgery. 2015;7(2):118–125. [PubMed: 24480728]
8. Oliver AA, Carlson KD, Bilgin C, et al. Bioresorbable flow diverters for the treatment of intracranial aneurysms: review of current literature and future directions. Journal of NeuroInterventional Surgery. 2022.

9. Oliver AA, Sikora-Jasinska M, Demir AG, Guillory RJ II. Recent advances and directions in the development of bioresorbable metallic cardiovascular stents: Insights from recent human and in vivo studies. Acta Biomaterialia. 2021.
10. Jinnouchi H, Torii S, Sakamoto A, Kolodgie FD, Virmani R, Finn AV. Fully bioresorbable vascular scaffolds: lessons learned and future directions. Nature Reviews Cardiology. 2019;16(5):286–304. [PubMed: 30546115]
11. Cassese S, Byrne RA, Ndrepepa G, et al. Everolimus-eluting bioresorbable vascular scaffolds versus everolimus-eluting metallic stents: a meta-analysis of randomised controlled trials. The Lancet. 2016;387(10018):537–544.
12. Kang S-H, Chae I-H, Park J-J, et al. Stent thrombosis with drug-eluting stents and bioresorbable scaffolds: evidence from a network meta-analysis of 147 trials. JACC: Cardiovascular Interventions. 2016;9(12):1203–1212. [PubMed: 27262860]
13. Otsuka F, Pacheco E, Perkins LE, et al. Long-term safety of an everolimus-eluting bioresorbable vascular scaffold and the cobalt-chromium XIENCE V stent in a porcine coronary artery model. Circulation: Cardiovascular Interventions. 2014;7(3):330–342. [PubMed: 24895447]
14. Schaffer JE, Nauman EA, Stanciu LA. Cold drawn bioabsorbable ferrous and ferrous composite wires: an evaluation of in vitro vascular cytocompatibility. Acta biomaterialia. 2013;9(10):8574–8584. [PubMed: 22885027]
15. Haude M, Ince H, Kische S, et al. Sustained safety and clinical performance of a drug-eluting absorbable metal scaffold up to 24 months: pooled outcomes of BIOSOLVE-II and BIOSOLVE-III. EuroIntervention. 2017;13(4):432–439. [PubMed: 28504239]
16. Verheye S, Wlodarczak A, Montorsi P, et al. BIOSOLVE-IV-registry: Safety and performance of the Magmaris scaffold: 12-month outcomes of the first cohort of 1,075 patients. Catheterization and Cardiovascular Interventions. 2020.
17. Shen D, Qi H, Lin W, et al. PDLLA-Zn-nitrided Fe bioresorbable scaffold with 53-μm-thick metallic struts and tunable multistage biodegradation function. Science advances. 2021;7(23):eabf0614. [PubMed: 34088662]
18. Schaffer JE. Biodegradable alloy wire for medical devices. In: Google Patents; 2020.
19. Jamshidi M, Rajabian M, Avery MB, et al. A novel self-expanding primarily bioabsorbable braided flow-diverting stent for aneurysms: initial safety results. Journal of neurointerventional surgery. 2020;12(7):700–705. [PubMed: 31776171]
20. Dabir D, Feisst A, Thomas D, et al. Physical properties of venous stents: an experimental comparison. CardioVascular and Interventional Radiology. 2018;41(6):942–950. [PubMed: 29492633]
21. Sadasivan C, Fiorella D. Preliminary in vitro angiographic comparison of the flow diversion behavior of Evolve and Pipeline devices. Journal of neurointerventional surgery. 2020;12(6):616–620. [PubMed: 31723048]
22. Muram S, Corcoran R, Cooke J, et al. Immediate flow-diversion characteristics of a novel primarily bioresorbable flow-diverting stent. Journal of Neurosurgery. 2022;1(aop):1–7.
23. Nishi H, Ishii A, Ono I, et al. Biodegradable flow diverter for the treatment of intracranial aneurysms: a pilot study using a rabbit aneurysm model. Journal of the American Heart Association. 2019;8(20):e014074. [PubMed: 31583935]
24. Wang K, Yuan S, Zhang X, et al. Biodegradable flow-diverting device for the treatment of intracranial aneurysm: short-term results of a rabbit experiment. Neuroradiology. 2013;55(5):621–628. [PubMed: 23381018]
25. Nevzati E, Rey J, Coluccia D, et al. Biodegradable magnesium stent treatment of saccular aneurysms in a rat model-introduction of the surgical technique. Journal of visualized experiments: JoVE. 2017(128).
26. Grüter BE, Täschler D, Strange F, et al. Testing bioresorbable stent feasibility in a rat aneurysm model. Journal of neurointerventional surgery. 2019;11(10):1050–1054. [PubMed: 30852526]
27. Bowen PK, Drelich A, Drelich J, Goldman J. Rates of in vivo (arterial) and in vitro biocorrosion for pure magnesium. Journal of Biomedical Materials Research Part A. 2015;103(1):341–349. [PubMed: 24665048]

28. Sanchez AHM, Luthringer BJ, Feyerabend F, Willumeit R. Mg and Mg alloys: how comparable are in vitro and in vivo corrosion rates? A review. Acta biomaterialia. 2015;13:16–31. [PubMed: 25484334]

29. Bowen PK, Drelich J, Goldman J. A new in vitro–in vivo correlation for bioabsorbable magnesium stents from mechanical behavior. Materials Science and Engineering: C. 2013;33(8):5064–5070. [PubMed: 24094225]

30. Lin W, Qin L, Qi H, et al. Long-term in vivo corrosion behavior, biocompatibility and bioresorption mechanism of a bioresorbable nitrided iron scaffold. Acta biomaterialia. 2017;54:454–468. [PubMed: 28315492]

31. Zhao N, Zhu D. Endothelial responses of magnesium and other alloying elements in magnesium-based stent materials. Metallomics. 2015;7(1):118–128. [PubMed: 25363018]

32. Altes TA, Cloft HJ, Short JG, et al. Creation of saccular aneurysms in the rabbit: a model suitable for testing endovascular devices. American Journal of Roentgenology. 2000;174(2):349–354. [PubMed: 10658703]

33. Schaffer JE, Nauman EA, Stanciu LA. Cold-drawn bioabsorbable ferrous and ferrous composite wires: An evaluation of mechanical strength and fatigue durability. Metallurgical and Materials Transactions B. 2012;43(4):984–994.

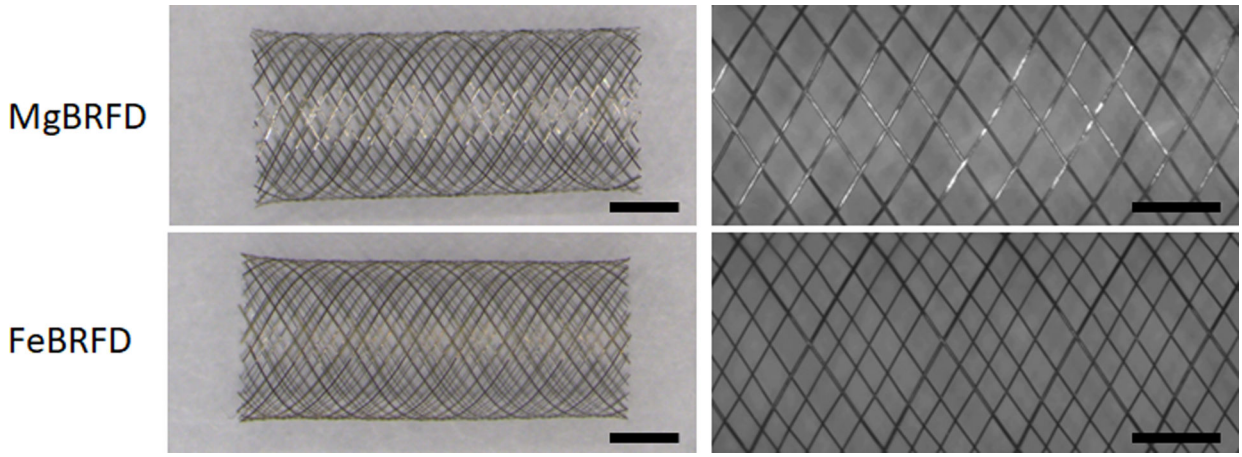

Figure 1:

Left) Macroscopic images of a MgBRFD and FeBRFD. Scale bars are 2 mm. **Right)** Representative 4X normal magnification images of a MgBRFD and FeBRFD used for porosity and pore density calculations. Scale bars are 1 mm.

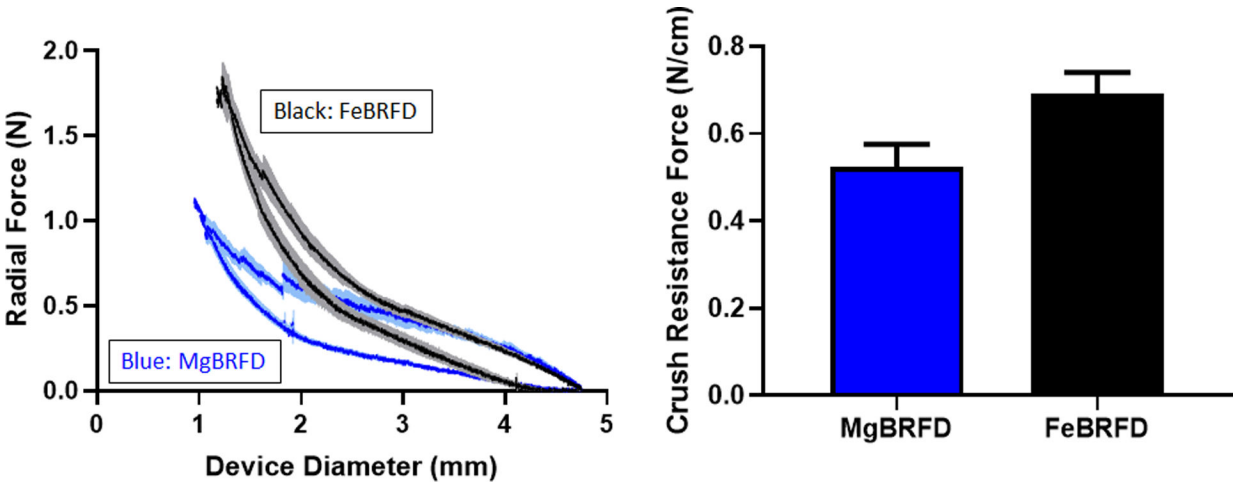

Figure 2:

Left) Radial force exerted by the MgBRFD and FeBRFDs versus device diameter during crushing and reexpansion between parallel plates. Solid lines and lighter shading represent the mean ± the standard error. **Right)** Crush resistance force for the MgBRFD and FeBRFDs.

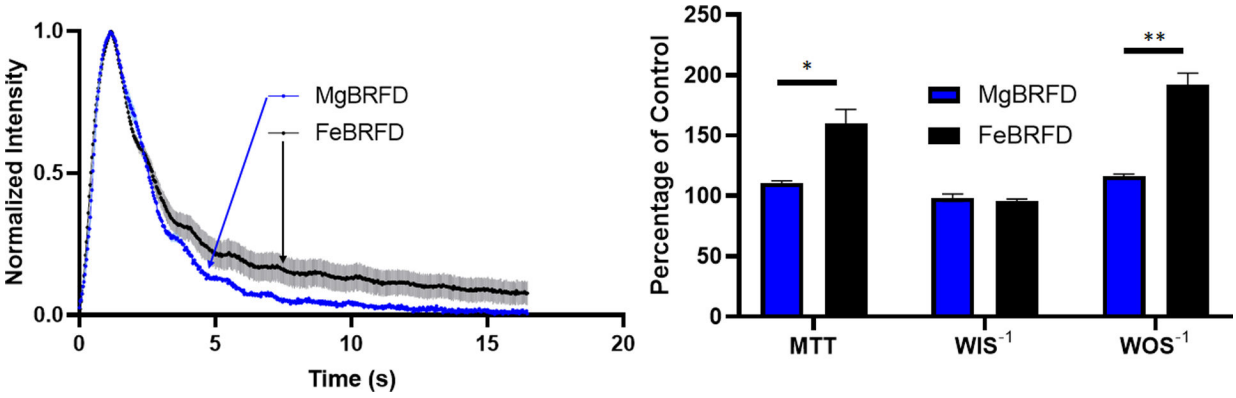

Figure 3:

Left) Normalized time density curves for the MgBRFD and FeBRFDs. Solid lines and lighter shading represent the mean ± the standard error. **Right)** Mean transit time (MTT), inverse wash-in slope (WIS^{-1}), and inverse wash-out slope (WOS^{-1}) for the MgBRFD and FeBRFDs presented as a percentage of the control condition. *$p < 0.05$, **$p < 0.005$

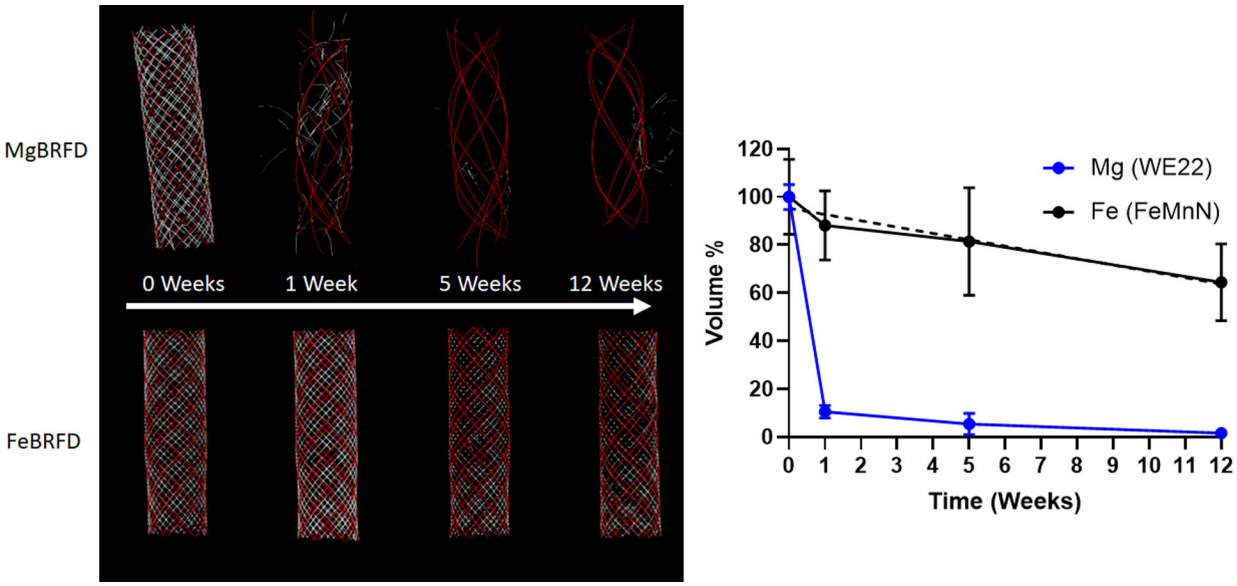

Figure 4:

Left) Representative MicroCT 3D renderings of the MgBRFD and FeBRFDs over time. For both devices, the red represents tantalum and white represents the bioresorbable wires. **Right)** Reduction in % volume of bioresorbable wires in the MgBRFD and FeBRFDs over time. The dashed line represents the linear line of best fit for the FeBRFD (R^2 = 0.934, p = 0.034)